



Light-induced rotation of dielectric microparticles around an optical nanofiber

GEORGIY TKACHENKO,^{1,6}  IVAN TOFTUL,²  CINDY ESPORLAS,¹  AILI MAIMAITI,^{1,3,4}
FAM LE KIEN,¹ VIET GIANG TRUONG,^{1,7}  AND SÍLE NIC CHORMAIC^{1,5,8} 

¹Okinawa Institute of Science and Technology Graduate University, Onna, Okinawa 904-0495, Japan

²Department of Physics and Engineering, ITMO University, Kronverkskiy prospekt 49197101, Saint-Petersburg, Russia

³Department of Physics, University College Cork, Cork, Ireland

⁴Current address: Department of Physics, Chalmers University of Technology, 412 96 Göteborg, Sweden

⁵Université Grenoble Alpes, CNRS, Grenoble INP, Institut Néel, 38000 Grenoble, France

⁶e-mail: georgiy.tkachenko@oist.jp

⁷e-mail: v.g.truong@oist.jp

⁸e-mail: sile.nicchormaic@oist.jp

Received 1 August 2019; revised 26 November 2019; accepted 9 December 2019 (Doc. ID 374441); published 14 January 2020

Evanescient electromagnetic fields near a waveguide can exert a transverse radiation force on scattering objects. To prove this experimentally, we demonstrate light-induced orbiting of isotropic, dielectric microparticles around an optical nanofiber that guides elliptically polarized, fundamental modes. The orbit frequency is proportional to the helicity of the coupled light. Interestingly, the observed motion is opposite to the energy flow circulation around the fiber. This result verifies the theoretically predicted negative optical torque on a sufficiently large particle in the vicinity of a nanofiber. © 2020 Optical Society of America under the terms of the [OSA Open Access Publishing Agreement](https://doi.org/10.1364/OPTICA.374441)

<https://doi.org/10.1364/OPTICA.374441>

Spin angular momentum (SAM) carried by paraxial free-space beams of light can be transferred to a material object, causing it to rotate around its axis (i.e., spin), if the object is absorbing or anisotropic [1]. In contrast, orbital angular momentum (OAM) in beams with optical vortices can even set isotropic, non-absorbing particles into rotation [2,3]. In nonparaxial light, SAM and OAM can couple, leading to, for example, orbiting of isotropic particles trapped by a tightly focused, nonvortex beam [4] and to observable, spin-dependent, transverse shifts of the light itself [5,6]. Symmetry breaking in a system consisting of a scattering object at the interface between two media, under oblique illumination, produces an interesting spin-dependent optomechanical effect [7].

Evanescient electromagnetic fields, which accompany total internal reflection and guiding of light, exhibit even more complicated spin-orbit interactions. In particular, aside from the common axial SAM associated with polarization, such fields exhibit a SAM component perpendicular to the wave vector [8]. In addition, a material object in an evanescent field can experience a transverse spin-dependent force, as demonstrated experimentally by means of a nanocantilever [9] or an optically trapped Mie scattering particle [10] placed near a total internal reflecting glass surface.

The evanescent field around an optical nanofiber [11] guiding a quasi-circularly polarized fundamental mode is also expected to carry significant OAM that is transferable to material objects [12]. In spite of numerous demonstrations of particle trapping, propulsion [13–15], and binding [16,17] in the vicinity of optical nanofibers, orbital motion of particles in such systems has never been reported in the literature. The main reason for this lack of experimental evidence was the uncertainty about the polarization of light at the waist of a nanofiber waveguide. This uncertainty has been lifted only recently [18–20]. In this Letter, we present a clear demonstration of the spin-dependent optical torque by means of light-induced orbiting of isotropic microspheres around a single-mode optical nanofiber.

Let us consider the interaction between a spherical, dielectric particle (of radius R_p) and the evanescent field of a single-mode optical nanofiber (of radius R_f), as sketched in Fig. 1(a). The electric part of an *elliptically* polarized guided mode is

$$\mathcal{E} = \left(\sqrt{1 + \sigma} \mathcal{E}_{p=+1} + e^{i\phi} \sqrt{1 - \sigma} \mathcal{E}_{p=-1} \right) / \sqrt{2}, \quad (1)$$

where $\sigma \in [-1, 1]$ is the helicity parameter [6], $\phi \in [0, 2\pi]$ determines the orientation of the symmetry axes of the polarization ellipse in the xy plane, and $\mathcal{E}_p = (e_r \hat{x} + p e_\phi \hat{\phi} + e_z \hat{z}) e^{i\beta z + ip\phi}$ is the electric part of the *quasi-circularly* polarized guided mode with a polarization rotation index $p = \sigma/|\sigma| = \pm 1$ [21]. Here, β is the propagation constant, and e_r , e_ϕ , and e_z are the cylindrical components of the mode-profile function of \mathcal{E}_p with $p = +1$. The azimuthal component of the Poynting vector of the elliptically polarized guided mode is $S_\phi = \sigma (e_z h_r^* - e_r h_z^*)/2$, where h_r and h_z are the components of the mode-profile function of the magnetic part, \mathcal{H}_p , of the guided mode with the polarization index $p = +1$. Since the longitudinal field components, e_z and h_z , are nonzero, we have $S_\phi^{(p)} \equiv S_\phi|_{\sigma=p} = p (e_z h_r^* - e_r h_z^*)/2 \neq 0$. It has been shown that $S_\phi^{(p=+1)} > 0$ and $S_\phi^{(p=-1)} < 0$ outside the nanofiber [21].

The light-induced force and torque on any object can be calculated if one knows the exact incident and scattered electromagnetic

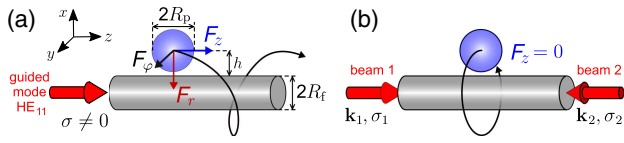


Fig. 1. (a) Isotropic, dielectric particle in the evanescent field of an elliptically polarized, fundamental mode of an optical nanofiber. Due to the azimuthal optical force, F_ϕ , the particle can rotate around the fiber. (b) We eliminate axial motion by using two counterpropagating beams with identical intensity profiles and opposite helicities, $\sigma_1 = -\sigma_2$.

waves. In our problem, the incident wave (here, the evanescent field) is well known [22]. Following the generalized Lorenz–Mie theory, the incident field can be decomposed into vector spherical harmonics, and the scattered field is thus found by application of boundary conditions [23,24]. Thence, the force and torque, respectively, can be found by integration of the linear and angular momenta over a surface enclosing the object. Note that although Lorenz–Mie theory is a generally accepted and fairly accurate semi-analytical approach to optomechanical calculations, it does not take into account multiple rescattering in the light–matter system.

The optical force exerted on a scattering particle near a nanofiber can be decomposed into the axial (F_z), radial (F_r), and azimuthal (F_ϕ) components [21] [see Fig. 1(a)]. Under F_r , the particle is attracted to the fiber surface and stays at $r = \sqrt{x^2 + y^2} \geq (R_f + R_p)$ (the inequality being due to surface roughness and Brownian motion). In this work, we aim at detection of the azimuthal force, F_ϕ , which sets the particle into orbital motion around the fiber. Since Brownian motion breaks mechanical contact between the particle and the fiber, the contribution from light-induced spinning of the particle to its azimuthal motion is expected to be negligible. According to our calculations, F_ϕ is much smaller than the axial force, F_z , which propels the particle towards $z > 0$. In order to prevent F_z from hindering detection of the light-induced rotation, we eliminate the axial motion by launching a second HE₁₁ mode propagating towards $z < 0$ into the nanofiber, with a power equal to that of the initial mode. This is realized experimentally by coupling two non-interfering (due to the lack of spatial coherence) laser beams into the opposite pigtailed of the tapered fiber [see Fig. 1(b)], where $\mathbf{k}_{1,2}$ are the wave vectors.

In principle, the rotation under F_ϕ could be studied if beam 1 were elliptically polarized ($\sigma_1 = \sigma \neq 0$) and beam 2 were linearly polarized ($\sigma_2 = 0$). However, such a beam 2 would produce a mode with an axially asymmetric intensity profile [25], and the particle would tend to stop at the “hot spots,” unless $|\sigma_1| \approx 1$. Since we consider the complete spectrum of σ , we set the polarization of beam 2 to also be elliptical, with $\sigma_2 = -\sigma_1$. In this case, the total azimuthal force is the sum of the contributions from both beams.

Once F_ϕ is known, the orbiting frequency of the particle at equilibrium can be easily calculated from the force balance equation, $F_\phi + F_{\text{fr}} = 0$, where F_{fr} is the friction. In our experiments, the particle is immersed in water, which produces a friction of $F_{\text{fr}} = -\gamma v$, where v is the linear velocity of the particle’s center, and γ is the drag coefficient. As demonstrated by Marchington *et al.* [26], an appropriate description of the friction for a microsphere in the evanescent field can be obtained using the lubrication correction [27] $\gamma = \gamma_0[(8/15)\ln(h/R_p - 1) - 0.9588]$, where $\gamma_0 = 6\pi\eta R_p$ is the Stokes drag, η is the dynamic viscosity of the fluid ($\eta \approx 1$ mPas for water at room temperature), and the distance

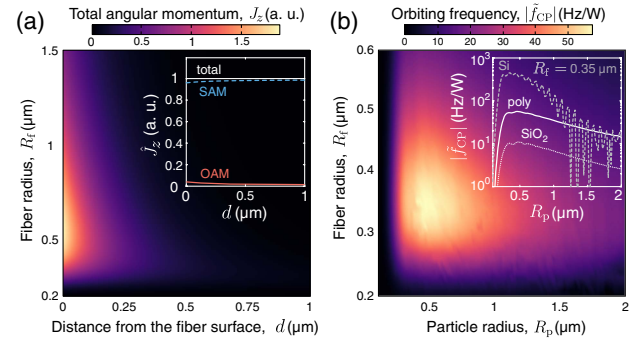


Fig. 2. Simulation results. (a) Density of the total angular momentum of light near a nanofiber (in water) guiding a fundamental mode with $\sigma = 1$. Inset: total angular momentum per photon and its orbital and spin components. (b) Orbiting frequency for a polystyrene particle, as a function of radii of the particle and the fiber. Inset: frequency at the optimum fiber radius ($R_f = 0.35 \mu\text{m}$) for three different particle materials: silicon, polystyrene, and silica.

$h = r - R_f$ [see Fig. 1(a)] depends on the particle surface roughness. We note that the above formula for γ is valid only for large enough particles, $R_p > 0.25 \mu\text{m}$ [27]. The absolute value of the particle rotation frequency around a fiber when both beams are circularly polarized (CP) can thus be expressed as

$$|f_{\text{CP}}| = |v|/[2\pi(b + R_f)] = |F_\phi|/[2\pi\gamma(b + R_f)]. \quad (2)$$

As follows from our simulations, in the general case of elliptical polarization (EP), the azimuthal force and the corresponding frequency, f_{EP} , are proportional to $\sigma = \sigma_1$, with opposite signs:

$$f_{\text{EP}} = -\sigma|f_{\text{CP}}|. \quad (3)$$

This result is consistent with the theoretical findings of Le Kien and Rauschenbeutel [21], for the relevant range of the size parameter, $n_m k R_p$, where n_m is the refractive index of the medium. For convenience, we normalize the rotation frequency by the total optical power, P . That is, we use $\tilde{f}_{\text{CP,EP}} = f_{\text{CP,EP}}/P$.

Our theoretical findings are summarized in Fig. 2, where J_z is the z component of the total angular momentum carried by the field near an optical nanofiber. In order to better understand the structure of angular momentum, we calculated the SAM and OAM densities [see the inset in Fig. 2(a)] using the canonical expressions [28,29]. Although the majority of J_z comprises the spin part, both components of the total angular momentum can contribute to orbital motion of particles in the vicinity of a nanofiber [30]. As shown in Fig. 2(b), the orbiting frequency is expected to reach about 57 Hz/W for a 1- μm (in diameter) polystyrene particle. As one can see in the inset, the maximum frequency scales with the refractive index: it equals 11 Hz/W for silicon dioxide ($n = 1.45$) and 450 Hz/W for silicon ($n = 3.67$). In practice, one should also consider the Brownian motion, which is inversely proportional to R_p : smaller particles would exhibit longer thermal displacements and therefore a weaker interaction with the evanescent field, which decreases dramatically with the distance from the fiber, d . As a reasonable compromise, we chose to use polystyrene beads with a diameter $2R_p = 3 \mu\text{m}$. Under these conditions, the expected frequency for CP input is $|\tilde{f}_{\text{CP}}| \approx 21.2$ Hz/W.

Our experimental setup is sketched in Fig. 3(a). The nanofiber is fabricated by controlled heating and pulling [31] of a step-index single-mode optical fiber (SM980G80 by Thorlabs, Inc.).

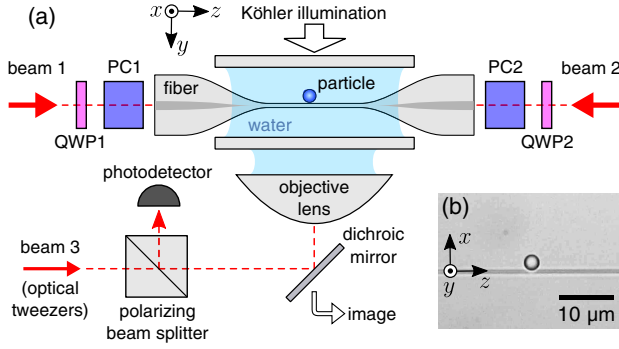


Fig. 3. (a) Experimental setup (not to scale): once the polarization transformations in the tapered fiber are reversed by the polarization compensators, PC1 and PC2, we set the values of σ_1 and $\sigma_2 = -\sigma_1$, by rotating the quarter-wave plates, QWP1 and QWP2. (b) Transmission image of a 3- μm polystyrene particle optically captured at the waist of a nanofiber.

The small tapering angles of 3 mrad provide adiabatic coupling [32,33] between the fundamental modes in the fiber pigtailed and those in the 2-mm-long cylindrical waist region having a radius of $R_f = 0.33 \pm 0.04 \mu\text{m}$ (measured over a set of five nanofibers). The fiber pigtailed are coupled to laser beams 1 and 2 from the same source (Ventus, Laser Quantum Ltd., emission wavelength $\lambda = 1.064 \mu\text{m}$). The initial linear polarization of the beams (along x and y for beams 1 and 2, respectively) is changed into elliptical by means of two quarter-wave plates, QWP1 and QWP2, with their slow axes oriented at equal angles, $\theta_{\text{QWP1}} = \theta_{\text{QWP2}} = \theta$, with respect to x , measured from the point of view of the receiver. This results in $\sigma = \sin 2\theta = -S_3$, where S_3 is the third Stokes parameter in beam 1.

A nanofiber sample is immersed into 0.3 mL of deionized water with 3- μm polystyrene particles (Phosphorex, Inc.) and sandwiched between two glass cover slips separated by 1.5-mm-thick spacers. The sample is imaged by a video camera (DCC3240C by Thorlabs, Inc.) through a water-immersion objective lens (Zeiss Plan-Apochromat, $63\times/1.00\text{w}$) under Köhler illumination [see Fig. 3(b)]. Individual particles are picked up from the bottom slip using an optical tweezers realized by focusing the collimated beam 3 (from the same laser) with the same objective lens. The polarizing beam-splitter cube transmits y -polarized beam 3 and is subsequently used for detection (Si amplified photodetector PDA10A2 by Thorlabs, Inc.) of the laser light escaping from the nanofiber due to scattering by the particle.

Due to uncontrolled bends, twists, or geometrical inhomogeneities, the fiber does not maintain polarization of guided light. In order to control the polarization state at the nanofiber waist, we reverse the unknown polarization transformations for both beams using two free-space compensators, PC1 and PC2. The compensation procedure described elsewhere [20] is based on self-scattering from the waist imaged by a second video camera, replacing the photodetector for this purpose.

Experimental results with $|\sigma| = 1$ are shown in Fig. 4. Orbital motion of the particle around the fiber causes clear quasi-periodical beatings of the measured voltage [see Fig. 4(a)]. The orbiting frequency, \tilde{f}_{CP} , scales linearly with optical power, as summarized in Fig. 4(b) for three different nanofibers. The data were fitted to Eq. (2) with an adjustable drag coefficient, γ_{fit} . The resultant frequency, $\tilde{f}_{\text{CP,fit}} = 19.2 \text{ Hz/W}$, is lower than the expected value

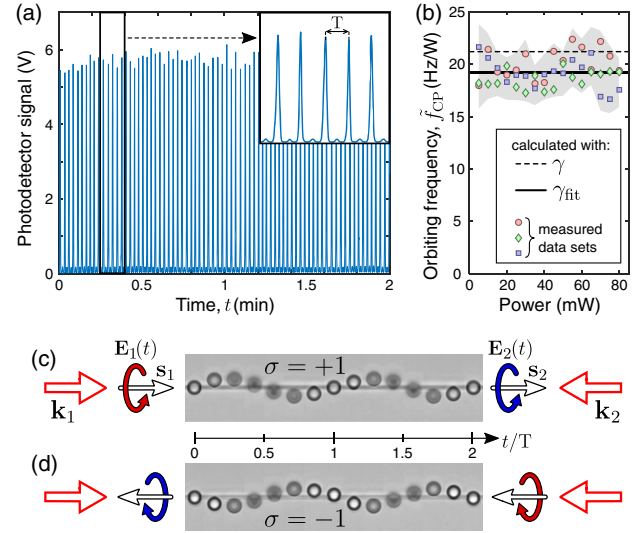


Fig. 4. Experimental results for a CP input ($R = \text{right}$, $L = \text{left}$). (a) Beatings in the detector signal acquired with an optical power of 15 mW in each beam. The zoomed-in view (inset) shows the local period, T . (b) Orbiting frequency versus power in each beam, at $\sigma = +1$. Markers: measured data sets for three samples; gray area: combined standard deviation range. Dashed line: frequency expected for the drag coefficient γ ; solid line: the best fit to the data with γ_{fit} . (c), (d) Time-lapse compilation of images for $\sigma = +1$ (c) and $\sigma = -1$ (d).

by about 9%, a small discrepancy given the complexity of the hydrodynamic problem, a complete solution of which is beyond the scope of this study.

When the sign of σ is reversed, the particle rotates in the opposite direction, with nearly the same period, T , as demonstrated by Visualization 1 and Visualization 2 and the corresponding time-lapse compilations of images in Figs. 4(c) and 4(d), where $\mathbf{s}_{i=1,2} = \sigma_i \mathbf{k}_i / k_i$, and the curved arrows denote the rotation of the electric field vector, \mathbf{E} , in the xy plane for each beam, from the point of view of the receiver. These arrows also indicate the circulation direction of the energy flow around the nanofiber [21].

The results for $\sigma \neq 1$ are presented in Fig. 5, where solid lines show the simulated frequency, $\tilde{f}_{\text{EP}}(\sigma)$, and each error bar is the standard deviation range for at least 20 T duration. For this data set, Eqs. (3) and (2) were applied, without adjustable parameters. As confirmed by Fig. 5(b), the transverse spin-dependent radiation force on the particle is proportional to the SAM projection on the propagation direction, with opposite sign. The observed light-induced rotation is antiparallel to the azimuthal component of the energy flow around the nanofiber [21]. This counterintuitive “negative” radiation torque (OAM-induced) is due to the dominant forward scattering. This is associated with multipolar interference in Mie scattering from large enough particles, $R_p > \lambda / (2\pi n_m) \approx 0.13 \mu\text{m}$. The associated forward scattering of light relates our findings to previous demonstrations of “negative” radiation forces [34–36].

Interestingly, σ influences not only the frequency, but also the particle’s trajectory. For CP input ($|\sigma| = 1$), it is close to a circle in the xy plane (see Visualization 1 and Visualization 2). When the polarization is elliptical ($|\sigma| < 1$), the trajectory acquires a figure-of-eight shape, with longer trips along z for smaller $|\sigma|$ (see Visualization 3). This distortion is due to the lack of axial symmetry in the intensity distribution for counterpropagating

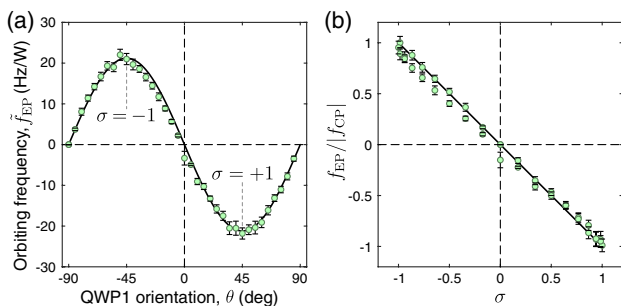


Fig. 5. Experimental results for an EP input and 15-mW power in each beam. (a), (b) Markers: measured orbiting frequency versus QWP1 orientation (a) or the \mathbf{k} -projection of SAM in beam 1 (b). Solid lines: simulation using Eq. (3), with $\sigma = \sin 2\theta$.

elliptically polarized modes [25]. Indeed, for $|\sigma|$ close to zero, the intensity maxima for beams 1 and 2 are aligned parallel to the x and y axes, respectively. Hence, the particle is accelerated towards $z > 0$ or $z < 0$ when passing through the xz or yz planes.

Here, we presented a clear experimental demonstration of a transverse, spin-dependent radiation force acting on material objects in evanescent electromagnetic fields. In contrast to previous studies on the subject, we used optical nanofibers, which provide extraordinarily clean experimental conditions, with high visibility and repeatability of measurements. An indispensable prerequisite of this experiment was the complete polarization control of light at the nanofiber waist. In addition to its use for verification of the above fundamental concept, the examined microparticle–nanofiber system could find an application in microfluidics, e.g., as an optically addressed rotary pump.

Funding. Okinawa Institute of Science and Technology Graduate University; Japan Society for the Promotion of Science (P18367); Russian Foundation for Basic Research (19-31-27001).

Acknowledgment. We thank J. M. Ward and K. Karlsson for managing the fiber pulling rig.

REFERENCES

1. M. E. J. Friese, T. A. Nieminen, N. R. Heckenberg, and H. Rubinsztein-Dunlop, *Nature* **394**, 348 (1998).
2. A. T. O’Neil, I. MacVicar, L. Allen, and M. J. Padgett, *Phys. Rev. Lett.* **88**, 053601 (2002).
3. V. Garcés-Chávez, D. McGloin, M. J. Padgett, W. Dultz, H. Schmitzer, and K. Dholakia, *Phys. Rev. Lett.* **91**, 093602 (2003).
4. Y. Zhao, J. S. Edgar, G. D. M. Jeffries, D. McGloin, and D. T. Chiu, *Phys. Rev. Lett.* **99**, 073901 (2007).

5. N. B. Baranova, A. Y. Savchenko, and B. Y. Zel’dovich, *JETP Lett.* **59**, 232 (1994).
6. K. Y. Bliokh, Y. Gorodetski, V. Kleiner, and E. Hasman, *Phys. Rev. Lett.* **101**, 030404 (2008).
7. S. Sukhov, V. Kajorndejnukul, R. R. Naraghi, and A. Dogariu, *Nat. Photonics* **9**, 809 (2015).
8. K. Y. Bliokh, A. Y. Bekshaev, and F. Nori, *Nat. Commun.* **5**, 3300 (2014).
9. M. Antognozzi, C. R. Bermingham, R. L. Harniman, S. Simpson, J. Senior, R. Hayward, H. Hoerber, M. R. Dennis, A. Y. Bekshaev, K. Y. Bliokh, and F. Nori, *Nat. Phys.* **12**, 731 (2016).
10. L. Liu, A. Di Donato, V. Ginis, S. Kheifets, A. Amirzhan, and F. Capasso, *Phys. Rev. Lett.* **120**, 223901 (2018).
11. L. Tong, F. Zi, X. Guo, and J. Lou, *Opt. Commun.* **285**, 4641 (2012).
12. F. Le Kien, V. I. Balykin, and K. Hakuta, *Phys. Rev. A* **73**, 053823 (2006).
13. G. Brambilla, G. S. Murugan, J. S. Wilkinson, and D. J. Richardson, *Opt. Lett.* **32**, 3041 (2007).
14. L. Xu, Y. Li, and B. Li, *New J. Phys.* **14**, 033020 (2012).
15. A. Maimaiti, V. G. Truong, M. Sergides, I. Gusachenko, and S. Nic Chormaic, *Sci. Rep.* **5**, 9077 (2015).
16. M. C. Frawley, I. Gusachenko, V. G. Truong, M. Sergides, and S. Nic Chormaic, *Opt. Express* **22**, 16322 (2014).
17. A. Maimaiti, D. Holzmann, V. G. Truong, H. Ritsch, and S. Nic Chormaic, *Sci. Rep.* **6**, 30131 (2016).
18. F. Lei, G. Tkachenko, J. M. Ward, and S. Nic Chormaic, *Phys. Rev. Appl.* **11**, 064041 (2019).
19. M. Joos, A. Bramati, and Q. Glorieux, *Opt. Express* **27**, 18818 (2019).
20. G. Tkachenko, F. Lei, and S. Nic Chormaic, *J. Opt.* **21**, 125604 (2019).
21. F. Le Kien and A. Rauschenbeutel, *Phys. Rev. A* **88**, 063845 (2013).
22. F. Le Kien, T. Busch, V. G. Truong, and S. Nic Chormaic, *Phys. Rev. A* **96**, 023835 (2017).
23. J. P. Barton, D. R. Alexander, and S. A. Schaub, *J. Appl. Phys.* **64**, 1632 (1988).
24. E. Almaas and I. Brevik, *J. Opt. Soc. Am. B* **12**, 2429 (1995).
25. F. Le Kien, J. Q. Liang, K. Hakuta, and V. I. Balykin, *Opt. Commun.* **242**, 445 (2004).
26. R. F. Marchington, M. Mazilu, S. Kuriakose, V. Garcés-Chávez, P. J. Reece, T. F. Krauss, M. Gu, and K. Dholakia, *Opt. Express* **16**, 3712 (2008).
27. G. P. Krishnan and D. T. Leighton, *Phys. Fluids* **7**, 2538 (1995).
28. K. Y. Bliokh, A. Y. Bekshaev, and F. Nori, *Phys. Rev. Lett.* **119**, 073901 (2017).
29. M. F. Picardi, K. Y. Bliokh, F. J. Rodríguez-Fortuño, F. Alpegiani, and F. Nori, *Optica* **5**, 1016 (2018).
30. F. Le Kien, T. Busch, V. G. Truong, and S. Nic Chormaic, *Opt. Express* **27**, 15046 (2019).
31. J. M. Ward, A. Maimaiti, V. H. Le, and S. Nic Chormaic, *Rev. Sci. Instrum.* **85**, 111501 (2014).
32. J. D. Love, W. M. Henry, W. J. Stewart, R. J. Black, S. Lacroix, and F. Gonther, *IEE Proc. J—Optoelectron.* **138**, 343 (1991).
33. Y. Jung, G. Brambilla, and D. J. Richardson, *Opt. Express* **16**, 14661 (2008).
34. S. Sukhov and A. Dogariu, *Phys. Rev. Lett.* **107**, 203602 (2011).
35. J. Chen, J. Ng, Z. Lin, and C. T. Chan, *Nat. Photonics* **5**, 531 (2011).
36. C. E. M. Démoré, P. M. Dahl, Z. Yang, P. Glynn-Jones, A. Melzer, S. Cochran, M. P. MacDonald, and G. C. Spalding, *Phys. Rev. Lett.* **112**, 174302 (2014).